

ULRR

FBG array arrangement optimization for impact localization

Item Type	Article
Authors	Duan, Chao;Cao, Jian;Wang, Hui;Yan, Xiaojian;Tian, Ye;Lewis, Elfed;Zhang, Jianzhong
Citation	Measurement Science and Technology, 2024, 35 (2), 025206
Publisher	IOP Publishing
Download date	2026-03-13 14:15:51
Item License	https://creativecommons.org/licenses/by-nc-sa/4.0/
Link to Item	https://doi.org/10.34961/researchrepository-ul.24598641



ACCEPTED MANUSCRIPT

FBG array arrangement optimization for impact localization

To cite this article before publication: Chao Duan *et al* 2023 *Meas. Sci. Technol.* in press <https://doi.org/10.1088/1361-6501/ad0b69>

Manuscript version: Accepted Manuscript

Accepted Manuscript is “the version of the article accepted for publication including all changes made as a result of the peer review process, and which may also include the addition to the article by IOP Publishing of a header, an article ID, a cover sheet and/or an ‘Accepted Manuscript’ watermark, but excluding any other editing, typesetting or other changes made by IOP Publishing and/or its licensors”

This Accepted Manuscript is © 2023 IOP Publishing Ltd.



During the embargo period (the 12 month period from the publication of the Version of Record of this article), the Accepted Manuscript is fully protected by copyright and cannot be reused or reposted elsewhere.

As the Version of Record of this article is going to be / has been published on a subscription basis, this Accepted Manuscript will be available for reuse under a CC BY-NC-ND 3.0 licence after the 12 month embargo period.

After the embargo period, everyone is permitted to use copy and redistribute this article for non-commercial purposes only, provided that they adhere to all the terms of the licence <https://creativecommons.org/licenses/by-nc-nd/3.0>

Although reasonable endeavours have been taken to obtain all necessary permissions from third parties to include their copyrighted content within this article, their full citation and copyright line may not be present in this Accepted Manuscript version. Before using any content from this article, please refer to the Version of Record on IOPscience once published for full citation and copyright details, as permissions may be required. All third party content is fully copyright protected, unless specifically stated otherwise in the figure caption in the Version of Record.

View the [article online](#) for updates and enhancements.

FBG array arrangement optimization for impact localization

Chao Duan¹, Jian Cao², Hui Wang², Xiaojian Yan², Ye Tian^{1,2,*}, Elfed Lewis³, Jianzhong Zhang^{1,*}

¹ Key Lab of In-Fiber Integrated Optics of Ministry of Education, Harbin Engineering University, Harbin, China

² Fiber Optical Sensing Center for Excellence, Yantai Research Institute & Graduate School, Harbin Engineering University, Yantai, China

³Optical Fibre Sensors Research Centre, Department of Electronic and Computer Engineering, University of Limerick, Limerick, Ireland

E-mail: field512@hrbeu.edu.cn; zhangjianzhong@hrbeu.edu.cn

Received xxxxxx

Accepted for publication xxxxxx

Published xxxxxx

Abstract

A method to optimize the arrangement location of the fiber Bragg grating (FBG) array is described to address the need to improve the accuracy of impact localization for aerospace vehicles. The sensitive area of the FBG, which is approximately elliptical, is analyzed using finite element simulation and experimental measurement. Based on this analysis, three optimized FBG sensing unit arrangements are proposed to improve the coverage of the FBG sensitive area at the center, side and corner positions, respectively. By employing the inverse problem analysis method in multiple repetitions of impact localization experiments, the accuracy of impact localization is improved from 74% with the traditional 4-corner arrangement to 84%, 88%, and 91% respectively for three arrangements, showcasing the effectiveness of the optimized FBG array arrangement method.

Keywords: Impact localization, FBG Sensitive Area, Sensors arrangement

1. Introduction

Aerospace vehicles are highly complex mechanical systems that have a significant value, high maintenance costs, and are susceptible to damage from various objects during their use [1]. Low-velocity impacts, although they may not leave visible marks, can accumulate and cause damage to the internal structure, leading to a serious decrease in structural strength [2-4]. This poses a significant safety risk for aerospace vehicles. By monitoring the impact location, the initial damage location can be determined, improving the efficiency of inspection and repair.

Currently, there are two main methods used to identify impact location. The first method involves using information such as the time difference and propagation speed of acoustic waves generated by the impact to localize the impact using

different sensors. However, this method is susceptible to reflection and scattering of the acoustic waves and requires sensors with good dynamic performance [5,6]. The second method is the inverse problem analysis method, where a sample model is created by arranging sensor arrays on the structure to be measured. The signal characteristics of different impact points are measured and compared with the sample model to determine the impact location [7]. The inverse problem analysis method is not affected by acoustic wave propagation and does not require sensors with high dynamic performance, making it an excellent method for impact localization. Commonly used positioning sensors include polyvinylidene fluoride sensors [8,9], piezoelectric sensors [10,11], fiber optic Fiber Bragg Grating (FBG) sensors [12-16], etc. Traditional electrical sensors have limitations such as difficulty in multiplexing, heavy cable weight, and susceptibility to electromagnetic interference,

which restrict their application in the aviation impact field. FBG sensors, on the other hand, have the advantages of high multiplexing capability, light weight, small size, and high interference immunity, making them well-suited for impact localization applications. The arrangement of the sensor array is crucial for accurately obtaining the signal characteristics of different impact points and directly impacts the monitoring accuracy [16].

Most of the existing methods for positioning impact loads on fiber optic FBG sensors use a square layout. For example, Du et al [12] placed four sensors at the four corners of a composite plate, achieving an average absolute error of 9.74 mm for impact point localization. Hirano et al [13] installed FBG strain sensors at the four corner positions of Carbon Fiber Reinforced Polymer reinforced panels, with high positioning accuracy in the frame direction arrangement. Shrestha et al [14] placed four FBG sensors along a 45° direction on the four corners of a composite plate, using an impact localization algorithm with error outliers and achieving an average error of about 20 mm. Jin et al [15] placed four sensors along the horizontal direction outside the detection area, using the martingale distance and impact point coordinates as inputs and outputs for an artificial neural network. Ding et al [16] arranged 8 FBGs in the center of 4 corners and 4 edges of a composite plate, using Db3-wavelet threshold noise reduction, the average error is 8.19 mm. Liu et al [17] installed 4 FBGs in the 4 corners of a composite plate, and designed a two-step localization method to achieve the collision localization, and the average error is 4.999 mm. Jiang et al [18] analyzed the effect of impact location and the number of sensors on the impact localization. The farther the impact location is from the sensors, the greater the attenuation of the stress wave is and the weaker the sensing signal is; with the sensing arrangement in the corner location, the average error of a single FBG sensor is 136.91 mm, two FBG sensors is 109.39 mm, three FBG sensors is 69.17 mm, and four FBG sensors was 16.18 mm. Wen et al [19] defined the sensitive range as a circle and used a genetic algorithm to optimize the FBG arrangement position with an average error of 21 mm. Jia et al [20] partitioned the monitored area into square hexagons of the same size, arranging a fiber optic FBG sensor in the center of each hexagon to improve localization accuracy. However, these methods approximate the sensitive area of the sensor as a simple shape, such as a square or polygon, whereas the actual sensitive shape of the FBG is an approximate ellipse [21]. This can result in some areas being less sensitive than others, leading to reduced average localization accuracy. Therefore, it is necessary to consider the sensitive characteristics of the fiber grating sensor itself when optimizing the arrangement of FBG positions.

In this paper, the arrangement method of FBG sensing array is optimized to improve the accuracy of impact localization based on the inverse problem analysis method

through the analysis of the approximately elliptical sensitive area of FBG sensors. The model allows for the determination of the approximately elliptical equal-strain sensitive area of an individual FBG sensing unit, which is then experimentally verified. Building upon the traditional four-corner arrangement method, the FBG array arrangement is optimized, resulting in the proposal of three arrangement modes that offer improved coverage of the areas to be monitored by the FBG sensitive area. Through the analysis of multiple repetitions of impact localization experiments, the impact accuracy is increased from 74% with the traditional four-corner arrangement to 84%, 88%, and 91% respectively, demonstrating the effectiveness of this method.

2. Principle

The inverse problem analysis method is used to determine the impact location by comparing the correlation of characteristic quantities between the sample model and the impact signal [22,23]. These characteristic quantities can be divided into two: frequency features and intensity features. The frequency features are related to the vibration modes excited by different impact locations, which can be represented by frequency distribution features specific to each location. The intensity features are related to the attenuation of waves during transmission, which varies with the distance between impact locations and each sensor, forming intensity distribution features specific to each location.

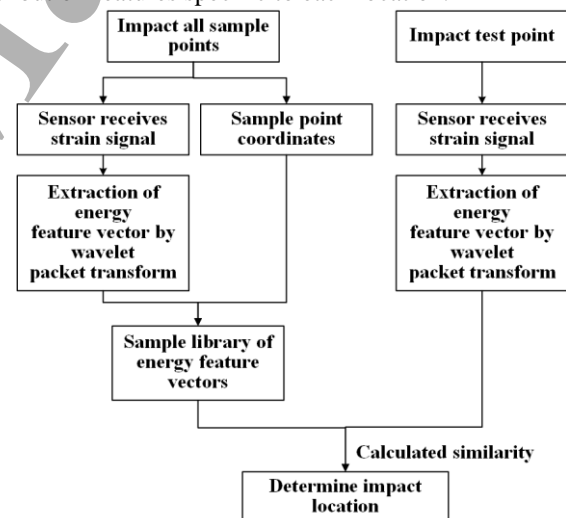


Fig. 1 Principle diagram of impact positioning

The impact localization process consists of three main components, as shown in Fig. 1. Firstly, a strain sensing array is installed on the plate that will be impacted, in order to monitor the strain caused by the impact. Next, sample points are divided on the plate and each sample point is impacted individually. The energy of the impact signal collected by the strain sensing array in each frequency band at each impact location is extracted using a wavelet packet transform to create an energy feature vector. This vector is used to build a sample

library. Finally, the impact localization is performed by extracting the impact energy vector, calculating its similarity with the sample library, and determining the impact location based on the sample with the highest similarity.

To measure the strain, an FBG was used as a strain sensor. The relationship between the axial strain and the shift in Bragg wavelength ($\Delta\lambda_B$) can be expressed using Eq. 1 [24].

$$\Delta\lambda_B = 2n_{eff}\Lambda[(1 - p_e)\varepsilon] \quad (\text{Eq. 1})$$

Where ε is the strain, n_{eff} is the effective refractive index of the core, and Λ is the grating period, $p_e = (n_{eff}^2/2)[p_{12} - \mu(p_{11} + p_{12})]$ is the effective elastic optical coefficient of the optical fiber (p_{11} , p_{12} are the elastic optical tensor components of the optical fiber material, μ is Poisson's ratio).

3. Simulation

The sensitivity characteristics of FBG to impact response were analyzed using Abaqus™ software. An aluminum alloy plate was used as the model for the impact, with a ball as the impact object, which is shown in Fig.2(a). The FBG sensor was placed on the back side of the plate. The plate had dimensions of 600mm × 600mm × 2mm, a Young's modulus of 70GPa, and a Poisson's ratio of 0.33. The ball had a diameter of 18mm, a Young's modulus of 210GPa, a Poisson's ratio of 0.25, and a density of 7.8g/cm³. The FBG size was $\Phi 0.125\text{mm} \times 10\text{mm}$, with a Young's modulus of 72GPa, a Poisson's ratio of 0.25, and a density of 2.3g/cm³. The rectangular frame area at the bottom of the plate is fixed. The ball was dropped from a predetermined height and impacted the stationary aluminum alloy plate. The FBG sensor measured the response in the form of the average value of the axial strain.

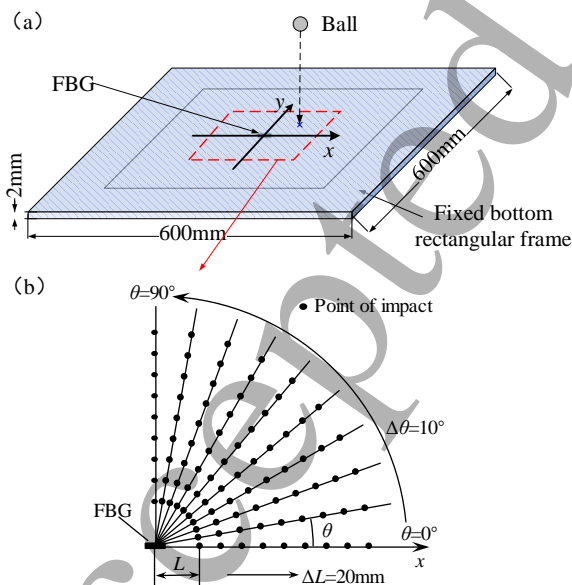


Fig. 2 Finite element analysis model.(a) model;(b) impact position

The impact positions on the aluminum alloy plate were analyzed to study the sensitivity of the FBG. Fig. 2(b) illustrates the impact position, with the FBG axial direction serving as the x-direction. The angle θ between the impact position and the center of the FBG, as well as the x-axis, was varied from 0° to 90° with a 10° interval. The distance L between the impact point and the FBG was varied from 40mm to 200mm with a 20mm interval in each direction. The ball was dropped from a height of 45 cm above the plate and impacted each point one by one. The strain experienced by the FBG after the impact varied with time, as depicted in Fig. 3(a). The maximum strain ε_m experienced by the FBG at different impact points was recorded. Fig3. (b) shows the trend of ε_m with L and θ . It can be observed that ε_m gradually decreases with increasing L and gradually increases with increasing θ .

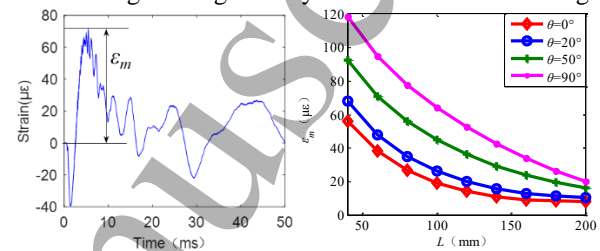


Fig. 3 FBG response in simulation (a) time domain signal; (b) relationship to impact location

Using $\varepsilon_m = 20, 30, 40\mu\varepsilon$ as reference values, the impact positions with the same ε_m at different angles were extracted. The FBG impact sensitivity range curves were plotted based on the test results from 0° to 90°, which were symmetrical about $x=0$ and $y=0$ due to the symmetry of their responses. Fig.4 shows these curves, where the shape of the sensitive area is approximately 'peanut' shaped. The long axis is perpendicular to the FBG axial direction, while the short axis is parallel to the FBG axial direction. The ratio of the long axis to the short axis gradually decreases as ε_m decreases.

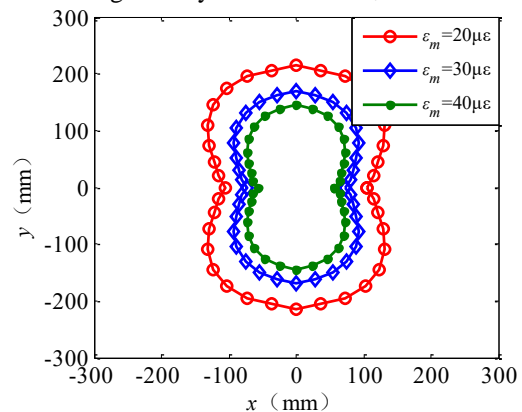


Fig. 4 Simulation of FBG sensitive range

4. Experimental Methodology and Measurements

4.1 Experimental platform construction

The impact positioning test system, as shown in Fig. 5(a),

comprises an aluminum alloy plate, a steel ball, a demodulator, and a computer. The aluminum alloy plate was made of 5A06 aluminum alloy with dimensions of 600mm×600mm×2mm and serves as the impacted object. The steel ball, made of 304 stainless steel, was of diameter 18mm and weighed 26g. It was used as the impactor. The demodulator (MOI-si155) has a sampling frequency of 1kHz and a wavelength range of 1470-1630nm with a wavelength resolution of ±3pm@1Hz. It was used to record the FBG wavelength variation. At the fixed edge, the Lamb wave generated by the impact will be reflected to interfere with the signal in the impact area, so only the 315mm×315mm area in the center of the aluminum alloy plate is selected as the impact area, and even if there is a reflected wave, it is easy to distinguish it in the time domain. The area is divided into an 8 × 8 equally spaced grid, with grid intersections as sample points of the impact and adjacent grid points spaced 45 mm apart. Each grid point is assigned a number, as shown in Fig. 5(b).

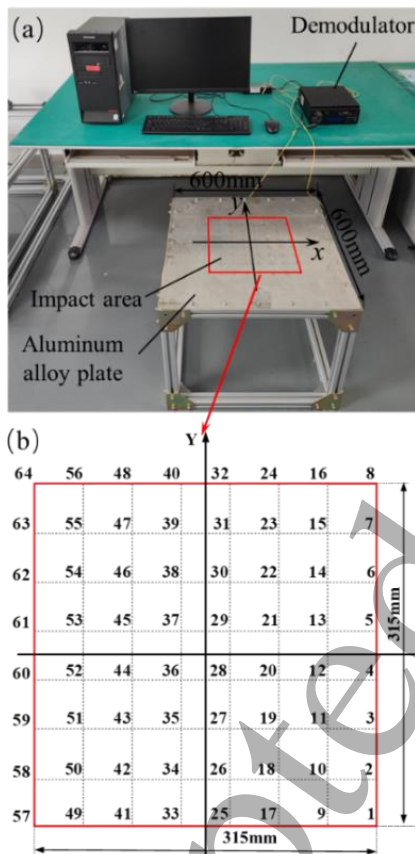


Fig. 5 Impact positioning test system (a) Physical diagram of the system (b) Schematic diagram of grid division

4.2 FBG Sensitive Area Analysis

The sensitivity characteristics of the FBG were investigated using the aforementioned test platform. The FBG sensor was positioned at the center of the back of an aluminum plate, and a steel ball was released from a height of 45 cm, striking the plate at the same location as shown in Fig. 2(b).

The shift in FBG wavelength was recorded using a demodulator, as shown in Fig. 6(a). The maximum wavelength shift, represented by λ_m , was measured for various impact points. Each point was impacted five times and the average value resulting from the five impacts was calculated. The trend of λ_m with respect to L at different θ angles was then plotted, as depicted in Fig. 6(b). It was observed that λ_m gradually decreases as L increases, and λ_m increases gradually as θ increases.

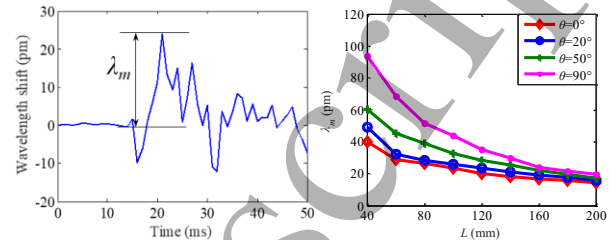


Fig. 6 FBG response in experiment (a) time domain signal; (b) relationship to impact location

Using $\lambda_m=20, 30,$ and 40pm as reference values, impact positions with the same ϵ_m (strain) were identified at different angles. The curves representing the FBG impact sensitivity range were plotted for angles ranging from 0 to 90°, after applying symmetry about the $x=0$ and $y=0$ axes due to the symmetrical nature of their responses. These curves, shown in Fig. 7, exhibit similar shapes to the Finite Element Analysis (FEA) results. The sensitive area can be approximated as a 'peanut' shape, with the long axis perpendicular to the FBG axial direction and the short axis parallel to the FBG axial direction. The ratio of the long axis to the short axis gradually decreases as λ_m decreases. When $\lambda_m=20\text{ pm}$, the long axis measures 195 mm, and the short axis measures 118 mm. The experimental and simulation results are slightly different. The reason for this may be related to the difference in material parameters, the difference in the details of the fix method and the loss of strain transfer in the experiment.

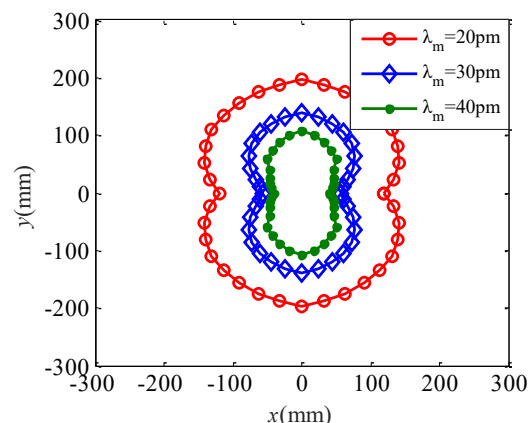


Fig. 7 Experimental of FBG sensitive range

4.3 FBG array arrangement scheme design

The monitoring area measures 315mm×315mm, and the $\lambda_m=20\text{pm}$ sensitive area can effectively cover 1/4 of the area, making it suitable for array division. The demodulator's wavelength resolution of 3pm ensures accurate measurements within this sensitive area. Based on the $\lambda_m=20\text{pm}$ sensitive area of FBG, the sensor arrangement is optimized and designed. Four FBG array arrangement modes are considered. Mode 1 is the traditional four-corner arrangement, with FBG sensors installed at the four corners at a 45° inclination angle (Fig. 8(a)), which served as a comparison group. Mode 2 builds upon Mode 1 by adding two sensors mouthed orthogonally to each other in the center position, expanding the coverage of the middle region and thus improving the measurement capability (Fig. 8(b)). Mode 3 rotates the four peripheral sensors by a certain angle to fully utilize the FBG's sensitive area and cover the measured area (Fig. 8(c)). Mode 4 focuses on the four corner positions while ensuring overall coverage of the impact area (Fig. 8(d)). The (X, Y, ϕ) next to each FBG in Fig. 8 indicates the FBG's position, with X representing the x-axis coordinate, Y representing the y-axis coordinate in mm, and ϕ indicating the angle between the FBG axial and x-axis in degrees.

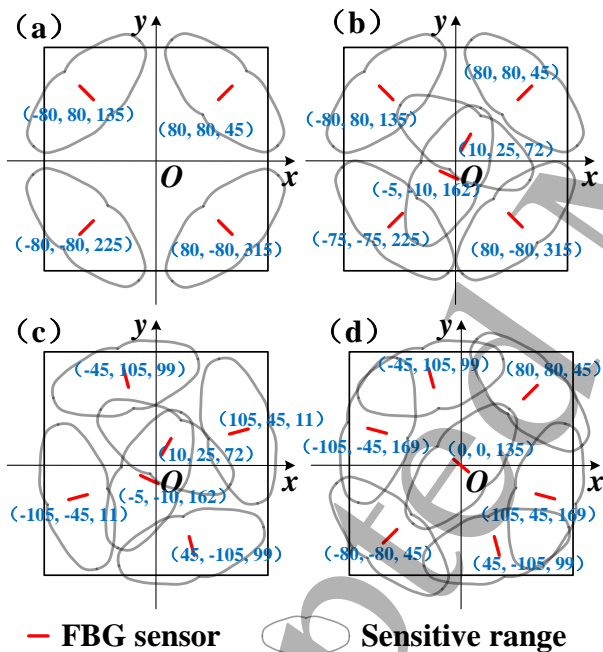


Fig. 8 Four layout mode (a) Mode 1; (b) Mode 2; (c) Mode 3; (d) Mode 4

Based on the above FBG arrangement scheme, all the required FBG sensors were arranged on the back of the aluminum plate. The schematic and physical drawings of the FBGs arrangement is shown in Fig. 9. A total of 13 FBGs are required, which are connected an optical fiber. The length of all FBGs is 10 mm and their wavelength and bandwidth are

shown in Tab. 1. The combination of FBGs was selected for each of the four layout modes, as defined in Tab. 2.

Tab. 1 Parameters of FBGs

FBG Number	1	2	3	4	5
Wavelength (nm)	1509.80	1515.97	1522.28	1528.03	1533.77
Bandwidth (nm)	0.296	0.287	0.289	0.302	0.301
FBG Number	6	7	8	9	10
Wavelength (nm)	1540.09	1546.06	1551.92	1558.12	1563.85
Bandwidth (nm)	0.319	0.297	0.317	0.284	0.313
FBG Number	11	12	13		
Wavelength (nm)	1570.08	1576.06	1582.23		
Bandwidth (nm)	0.304	0.312	0.306		

Tab. 2 Layout mode with FBG serial number

Mode	1	2	3	4
FBG Number	4, 7, 9, 13	2, 3, 4, 7, 9, 13	2, 3, 5, 8, 10, 12	1, 4, 6, 8, 9, 11, 12

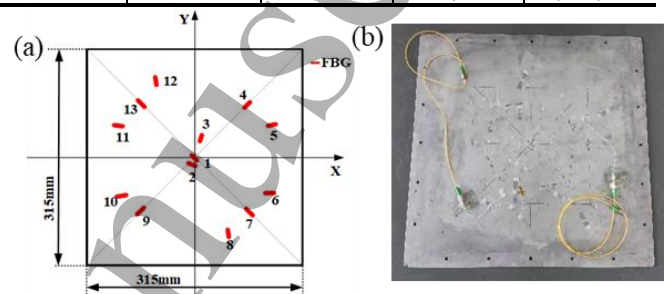


Fig. 9 FBG sensors arrangement (a) schematic; (b) physical

4.4 Impact positioning accuracy analysis

The experiment involved dropping a steel ball from a height of 45 cm and observing its impact on the 64 grid points. The wavelength changes of all FBGs were recorded using the FBG demodulator. This process was repeated five times and the data were processed using the method described in Section 2.2. Fig. 10(a) and (c) show the wavelength changes of FBG4 and FBG7 at impact point 1, while Fig. 10(b) and (d) show the corresponding energy feature vector. Each FBG at each impact position has a different energy feature vector. Based on Table 1, specific FBG combinations were selected to create a sample library for each arrangement mode.

The steel ball was then dropped from the same height its impact recorded at the 64 grid points. The responses of the FBGs were compared with the sample library to determine the impact locations. This process was repeated seven times to reduce errors caused by non-systematic factors. Different layout patterns were used to obtain the impact positions. Table 2 shows the results of the localization accuracy. A measured position was considered successful if it matched the actual impact position, and unsuccessful if it did not. The localization accuracy improved from 74% to 84%, 88%, and 91% when considering the sensitive area of the FBG and optimizing the sensing network arrangement. This improvement demonstrated the effectiveness of these considerations in enhancing the impact localization accuracy.

A detailed analysis of points that were not accurately located during a round of impact is shown in Fig. 11. Mode 1 exhibited the worst positioning accuracy, and the failure points are mostly distributed at the edge and middle of the impact area; Mode 2, after adding two FBG sensors in the middle, shows a significant improvement specifically the positioning accuracy in the middle area compared with Mode 1; Mode 3, after optimizing the FBG coverage, further improved the positioning accuracy compared with Mode 2; Mode 4 was focused on improving the positioning accuracy in the corner locations, as well as the upper left and lower right areas. The latter two were superimposed by locating two FBGs in the sensitive area, and the positioning accuracy in these two areas was significantly improved. The unsuccessfully located points were mostly concentrated in the locations not covered by the FBG sensitive area. So it is necessary to consider the FBG sensitive area and its coverage of the area to be detected in real measurement scenarios.

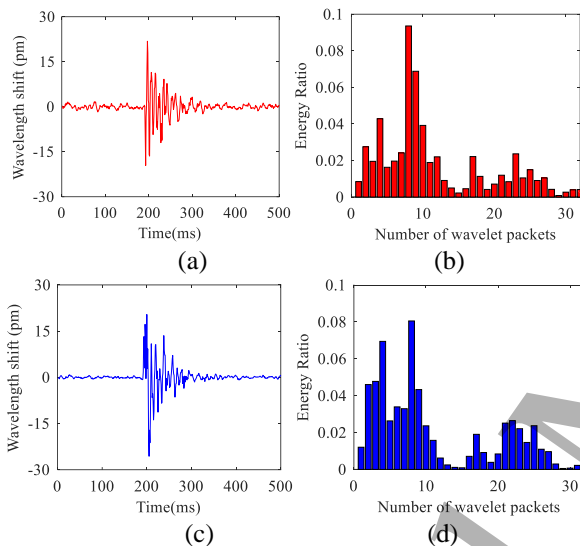


Fig. 10 The wavelength changes of FBG4(a) and FBG7(c), the energy feature vector of FBG4(b) and FBG7(d)

A detailed analysis was conducted on the points that were inaccurately located during an impact experiment, as shown in Fig. 11. It was observed that Mode 1 exhibited the lowest positioning accuracy, with most of the failure points located at the edges and middle of the impact area. Mode 2, which added two FBG sensors in the middle, demonstrated a significant improvement in positioning accuracy in the middle area compared to Mode 1. Mode 3, after optimizing the FBG coverage, showed further improvement in positioning accuracy compared to Mode 2. Mode 4, on the other hand, focused on improving the positioning accuracy in the corner location by having two overlapping FBG sensitive area, resulting in a significant improvement in positioning accuracy in these areas. It was observed that the points that were inaccurately located were mostly concentrated in the areas not covered by the FBG sensitive area. Hence, it is crucial to

consider both the FBG-sensitive area and its coverage within the targeted area.

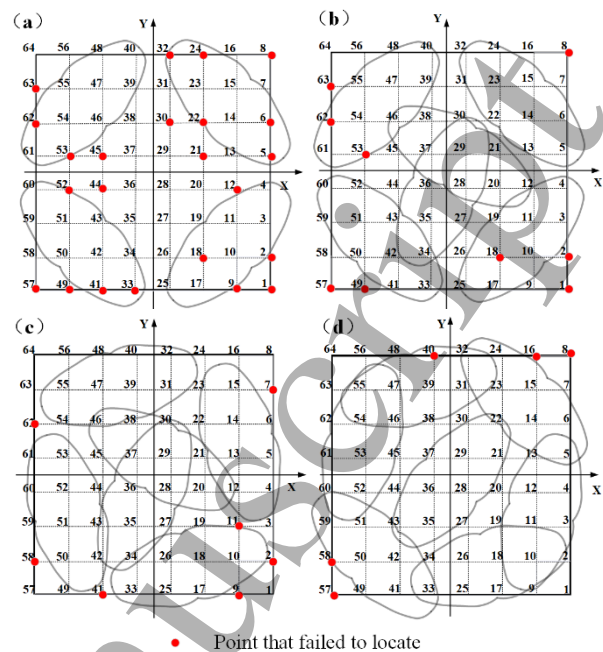


Fig. 11 Unsuccessfully located points (a)Mode 1; (b)Mode 2; (c)Mode 3; (d)Mode 4

To examine the impact of impact energy on FBG-sensitive area size, the impact height was varied to analyze its effect on the impact accuracy. Steel balls were dropped from heights of 30cm, 20cm, 10cm, and 5cm, striking 64 grid points sequentially. Each height was repeated 7 times, and positioning accuracy was recorded for different heights and FBG arrangement methods (as shown in Tab. 3). As the impact height decreases, localization accuracy gradually diminishes. This can be attributed to the decrease in impact energy, resulting in the inability of FBG sensors located further from the impact point to detect the signal effectively. However, in the case of the same impact height, Mode 1 exhibits the poorest localization accuracy, while the other three modes show approximately 5-18% improvement in localization accuracy due to the consideration of FBG sensitive area coverage. Mode 4, with the highest FBG-sensitive area coverage, demonstrates the highest improvement in localization accuracy.

Tab. 3 Impact location accuracy as a relationship between layout mode and impact height

Impact height (cm)	Impact location accuracy			
	Mode 1	Mode 2	Mode 3	Mode 4
45	74%	84%	88%	91%
30	57%	66%	71%	75%
20	55%	63%	67%	73%
10	51%	60%	61%	66%
5	28%	33%	35%	44%

5 Conclusion

A method has been described to optimize the arrangement of FBG array to improve the accuracy of impact localization. The method takes into consideration the sensitive characteristics of FBGs. Initially, a transient dynamics-based finite element analysis model of impact sensing is established. This model simulates the impact location near a separate FBG sensing unit at certain spatial intervals. The model also takes into account the equal strain sensitive area of the FBG, which is approximated to be an ellipse with a ratio of the long axis to the short axis close to 2:1. The short axis of the ellipse coincides with the axial direction of the FBG. This approximation was also verified through experimental measurement. Based on the traditional 4-corner arrangement, three optimized arrangement schemes are proposed to improve the coverage of the FBG sensitive area at the center, side and corner positions. These schemes aim to improve the coverage of the FBG-sensitive area to the impact zone. Multiple repetitions of impact localization experiments using the inverse problem analysis method were conducted. The results confirm that increasing the coverage of the sensitive area with strategically located FBGs effectively improves the accuracy of impact point identification. The localization accuracy is increased from 74% to 84%, 88%, and 91% for the three optimized arrangement schemes, respectively. The effect of impact energy reduction on the impact localization accuracy was also examined. It was observed that the impact accuracy decreases with the reduction of impact energy. However, the localization accuracy of the optimized arrangement model demonstrated an improvement in the range 5-18% at the same impact energy. Therefore, through a consideration of the sensitive area covered using strategically located FBGs and optimizing the sensing array arrangement can effectively improve the impact localization accuracy. This improvement is crucial for efficient failure detection in aero structures including spacecraft.

Acknowledgements

This work was supported in part by the National Natural Science Foundation of China (62005063); the Fundamental Research Funds of the Central (3072022JC2702); the National Key Research and Development Program of China (2021YFC2802202); Heilongjiang Natural Science Fund for Distinguished Young Scholars (JQ2022F001).

References

[1] Jeannot Frieden, Joel Cugnoni, John Botsis, et al. Low energy impact damage monitoring of composites using dynamic strain signals from FBG sensors - Part II: Damage identification. *Composite Structures*, 2012, 94(2): p. 593-600.

[2] Shi Y, Soutis C. Modelling low velocity impact induced damage in composite laminates. *Mechanics of Advanced Materials and*

Modern Processes, 2017, 3(1): p. 14-26.

[3] Christoforou A P, Yigit A S. Characterization of impact in composite plates. *Composite Structures*, 1998, 43(1): p. 15-24.

[4] Amoroso M P, Caneva C, Nanni F, et al. Acoustic Emission Performance for Damage Monitoring of Impacted FRP Composite Laminates. *Review of Progress in Quantitative Nondestructive Evaluation*, 2003(657): p. 1447-1454.

[5] Xu J, Deng J: Study on Lamb Wave Dispersion Curves for the Testing of Metal Plates. *Intelligent Computing, Networked Control, and Their Engineering Applications*, 2017: p. 324-332.

[6] Ciampa F, Meo M. Acoustic emission source localization and velocity determination of the fundamental mode $A(0)$ using wavelet analysis and a Newton-based optimization technique. *Smart Materials and Structures*, 2010, 19(4).

[7] Rezayat A, De Pauw B, Lamberti A, et al. Reconstruction of impacts on a composite plate using fiber Bragg gratings (FBG) and inverse methods. *Composite Structures*, 2016, 149: p. 1-10.

[8] Monkhouse R S C, Wilcox P D, Cawley P. Flexible interdigital PVDF transducers for the generation of Lamb waves in structures. *Ultrasonics*, 1997, 35(7): p. 489-498.

[9] Zeng F, Peng C, Liu Y, et al. Reactive Molecular Dynamics Simulations on the Disintegration of PVDF, FP-POSS, and Their Composite during Atomic Oxygen Impact. *Journal of Physical Chemistry A*, 2015, 119(30): p. 8359-68.

[10] PERELLI A, DEMARCHI L, MARZANI A, et al. Acoustic emission localization in plates with dispersion and reverberations using sparse PZT sensors in passive mode. *Smart Materials and Structures*, 2012, 21(2).

[11] GHAJARI M, SHARIF KHODAEI Z, ALIABADI M.H. Impact detection using artificial neural networks. *Key Engineering Materials*, 2011, p. 488-489(488).

[12] Du Liangya, Jiang Wensong, Luo Zai. Multi FBG sensor-based impact localization with a hybrid correlation interpolation method. *Measurement Science & Technology*, 2022, 33(7): p. 075002-1.

[13] N. Hirano, H. Mamizu, A. Kuraishi, et al. Detectability Assessment of Optical Fiber Sensor Based Impact Damage Detection for Composite Airframe Structures. *Ewshm European Workshop on Structural Health Monitoring*, 2014..

[14] Pratik Shrestha, Jin-Hyuk Kim, Yurim Park, et al. Impact localization on composite structure using FBG sensors and novel impact localization technique based on error outliers. *Composite Structures*, 2016, 142: p. 263-271.

[15] Jin Jing, Zhu Yunhong, Zhang Yibo, et al. Micrometeoroid and Orbital Debris Impact Detection and Location Based on FBG Sensor Network Using Combined Artificial Neural Network and Mahalanobis Distance Method. *Ieee Transactions on Instrumentation and Measurement*, 2021, 70.

[16] Ding G, et al. Localization of low velocity impact on CFRP laminate using normalized error outlier-based algorithm cooperating with Db3-wavelet threshold noise reduction and FBG sensors. *Optical Fiber Technology*, 80, 2023, p. 103455.

[17] Liu Q, et al. A two-step localization method using wavelet packet energy characteristics for low-velocity impacts on composite plate structures. *Mechanical Systems and Signal Processing*, 188, 2023, p. 110061.

[18] Jiang W, et al. Multi-fbg sensor array-based impact localization with an energy eigenvector. *Optical Engineering*, 61(6), 061406.

[19] Wen X, et al. Localization of low velocity impacts on CFRP laminates based on FBG sensors and BP neural networks. *Mechanics of Advanced Materials and Structures*, 2021, pp. 5478-5487.

[20] Hongyu Jia, Jie Zeng, etc. Research on Fiber Optic Impact Load Localization Based on Honeycomb Layout and Fractal Filtering Principle. *SPIE 10618, 2017 International Conference on Optical Instruments and Technology: Advanced Optical Sensors and*

1
2
3 Applications, 106180A (10 January 2018).

4 [21] Xiao-Su Y I , Jia L , Xiang-Yu Y E ,et al.An Optimal Placement
5 of FBG Sensor Network Based on Probability Model. Opto-
6 Electronic Engineering, 2013, 124: p. 1045-1048.

7 [22] Doebling S W.Damage Identification and Health Monitoring of
8 Structural and Mechanical Systems from Changes in Their Vibration
9 Characteristics:A Literature Review. Shock&Vibration Digest, 1996,
10 30(11): p. 2043-2049.

11 [23] Rezayat A,Pauw B D,Lamberti A,et al.Reconstruction of
12 impacts on a composite plate using fiber Bragg gratings(FBG)and
13 inverse methods. Composite Structures,2016(149): p. 1-10.

14 [24] Aydin R , Richard H , Hendriks R C ,et al.Calculation of the
15 Mean Strain of Smooth Non-Uniform Strain Fields Using
16 Conventional FBG Sensors.Journal of Lightwave Technology, 2018,
17 p. 1-1.
18
19
20
21
22
23
24
25
26
27
28
29
30
31
32
33
34
35
36
37
38
39
40
41
42
43
44
45
46
47
48
49
50
51
52
53
54
55
56
57
58
59
60